The evolution of sputtered iron nitride thin films under thermal treatment

D. H. Mosca, S. R. Teixeira, P. H. Dionisio, I. J. R. Baumvol, W. H. Schreiner, and W. A. Monteiro
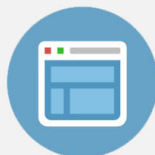
The evolution of sputtered iron nitride thin films under thermal treatment

D. H. Mosca, S. R. Teixeira, P. H. Dionisio, I. J. R. Baumvol, and W. H. Schreiner
Laboratório de Filmes Finos, Instituto de Física da UFRGS, 91500 Porto Alegre, Brazil

W. A. Monteiro
Instituto de Pesquisas Energéticas e Nucleares, CP 11049, 05508 São Paulo, Brazil

The thermal evolution of reactively sputtered iron nitride thin films has been investigated by x-ray diffraction, Mössbauer conversion electron spectroscopy, transmission electron microscopy, and magnetic measurements. The results show that, independently of the original nitrogen content of the films, a similar composition of the end products after the 500 °C annealings is reached, being all composed of α-Fe plus γ'-Fe$_4$N in a wide range of relative proportions. The magnetic characteristics, however, are different depending on the nitrogen content of the as-deposited films.

I. INTRODUCTION

The Fe-N system has many interesting magnetic and metallurgical properties. The initial interest in the nitriding of steels was mainly in improving surface hardness and wear resistance. More recently the iron nitrides reappeared in the literature but now as thin films and potential candidates for magnetic recording heads or eventually recording media. The Fe$_{16}$N$_2$ nitride can display a saturation magnetization even higher than pure Fe.[1] Several reports on Fe$_4$N particulates appeared in the literature.[2-6] These magnetic pigments have so far eluded the hope that Fe$_4$N particles would be much less susceptible to corrosion than are metal particles. Also high-magnetization Fe$_{16}$N$_2$ particulate media have not been realized, so far.

Within the still scarce thin film Fe-N literature one finds a trend towards ion beam assisted techniques for the deposition method. Several papers on ion beam assisted deposition (IBAD) appeared recently.[7-14] Also, very encouraging results have been obtained with the production of Fe/Fe$_x$N multilayers.[11] The magnetic characteristics of these thin film systems can be tailored apparently at will. Good anticorrosion properties of the nitride thin films were reported.

Somewhat less effort as compared to IBAD has been put into nitrogen ion implantation of thin iron films. We also find a good versatility of the method in the production of the various nitrides.[15,16]

The reactive sputtering deposition technique of thin films in contrast has received less attention. This is curious, since sputtering is a well-established industrial process, whereas the ion beam techniques still have to prove their industrial feasibility.

Kano *et al.*[17] prepared iron nitride films with a triode dc sputtering system. The analysis of the obtained films was based on magnetization measurements and was mainly of exploratory nature. The authors obtained indirect evidence of the Fe$_{16}$N$_2$ phase which is of high magnetization, but mainly found the Fe$_4$N and the nonferromagnetic Fe$_3$N and Fe$_2$N phases together with α-Fe.

Lo *et al.*[18,19] described the deposition of Fe$_x$N thin films with the rf diode sputtering method. This deposition method leads to high temperature substrate conditions, a determinant factor in the structure and magnetic behavior of the films. The authors showed the deposition of Fe$_4$N, α-Fe + Fe$_4$N and ϵ-Fe$_3$N depending on the Ar/N$_2$ ratio in the plasma composition. The film microstructure shows faceted, high surface area, thin films with crystallite sizes of 400–500 Å.

Chang *et al.*[20] reported on the rf diode sputter deposition of iron nitride thin films using negative substrate bias voltages. This negative bias, of course, leads to a lower substrate temperature due to lower electron impact but, on the other hand, involves Ar$^+$ and N$_2^+$ ions bombarding the substrate during deposition. They found various iron nitride compounds in the films, either single-or mixed-phase α-Fe, Fe$_4$N, and ϵ-Fe$_{2-3}$N. The films cover a wide range of magnetic properties appropriate for thin film magnetic heads and media. The control of all sputtering conditions was reported to be delicate.

Recently we[21] described the compositional and magnetic properties of high rate dc magnetron sputtered iron nitride thin films deposited under various Ar/N$_2$ ratios in the sputtering plasma. The experimental results included Auger spectroscopy, CEMS, x-ray and magnetic measurements. The main findings of that work showed that the nitrogen content of the Fe$_x$N films increases with the N$_2$ partial pressure in the deposition chamber, while the deposited films are appreciably phase inhomogeneous, a feature which leads to complicated x-ray and CEMS spectra. Furthermore, the magnetron sputtering always leads to Fe$_x$N films with relatively small saturation magnetization and moderate coercivities. The structure and magnetic behavior could be understood due to the low temperature deposition process typical of that technique.

This work concentrates on the evolution under thermal treatment of these sputter-deposited films. The interest in this type of work has two reasons: first, there is very little information on the phase evolution in the Fe$_x$N thin film system under thermal treatment and second, the sputtered films show new and interesting magnetic properties when annealed.

II. EXPERIMENT

The experimental conditions of sputter deposition of the $Fe_x N$ thin films were described earlier[21] as well as the experimental techniques used in the characterization of the films. We will refer this article to samples B, C, and D of Ref. 21.

The transmission electron microscope (TEM) analyses of the present work were carried out in diffraction, bright-field, and dark-field modes using a 200-kV electron microscope. The pictures of the samples were obtained by first dissolving the special KBr substrate used for the deposition in water.

The thermal annealing of the samples was sequential, in steps of 100 °C ending at 500 °C. The annealing was done for 1 h at each step in a high vacuum furnace at pressures of 1×10^{-7} Torr. After each step the samples were characterized by x-ray diffraction and conversion electron Mössbauer spectroscopy (CEMS), respectively. Some selected magnetic measurements employing a vibrating sample magnetometer (VSM) were also performed on the end products.

III. EXPERIMENTAL RESULTS

A. Mössbauer data

Figure 1 shows the CEMS spectra of sample B (partial pressure of nitrogen in the deposition chamber $P_{N2} = 4 \times 10^{-6}$ Torr) starting with the as-deposited one. We show only the results of the selected treatment temperatures of 300 and 500 °C which clearly evidence the evolution.
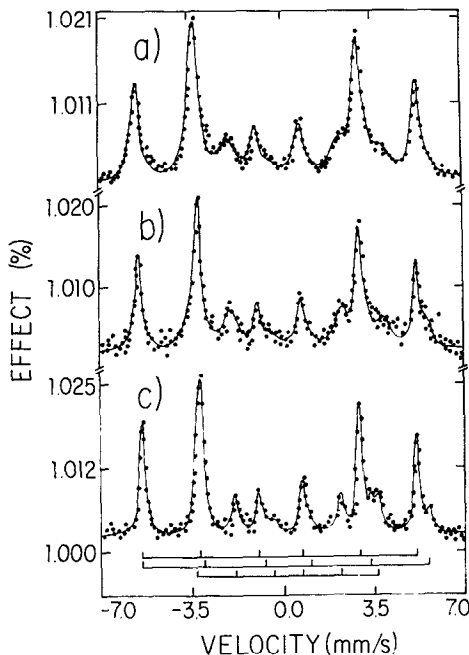

FIG. 1. CEMS spectra of sample B (partial pressure of nitrogen in the deposition chamber $P_{N2} = 4 \times 10^{-6}$ Torr) (a) as-deposited; and annealed at: (b) 300 °C; (c) 500 °C.

The spectrum of the as-deposited sample, Fig. 1(a), is dominated by the sextet of metallic α-Fe, displaying, however, very large linewidths. This spectrum also shows the presence of another magnetic component which cannot be identified. The larger linewidths obtained in the fitting (see Table I) are apparently due to a spreading in the magnitude of the magnetic hyperfine fields which normally come from a large disorder in the occupation of the interstitial nitrogen sites.[22] Figure 1(b) shows the CEMS result of the sample treated at 300 °C. Now, besides the α-Fe spectrum, the γ'-$Fe_4 N$ component can also be identified, although with a certain reserve since the hyperfine fields are somewhat larger than those found in the literature.[23] Finally, after the 500 °C treatment, the sample shows the spectrum of Fig. 1(c). This spectrum shows a phase mixture of α-Fe together with γ'-$Fe_4 N$, which can now be identified unambiguously. The relative spectral areas of Fe and $Fe_4 N$ are 60% and 40%, respectively. Table I shows the Mössbauer fitting parameters.

Figure 2 shows the Mössbauer results for sample C ($P_{N2} = 3 \times 10^{-5}$ Torr). The very complex spectrum 2a of the as-deposited sample is interpreted as a sum of the ferromagnetic $Fe_x N$ ($x > 3$) phase coexisting with paramagnetic ζ-$Fe_2 N$ deficient in nitrogen.[24] Figure 2(b) shows the sample after an anneal at 200 °C. Without better definition, the interpretation of the spectrum remains the same. A drastic change can be seen in sample C after the 300 °C anneal. The spectrum is now completely dominated by a paramagnetic compound, Fig. 2(c). We cannot decide on basis of the Mössbauer results which paramagnetic compound is involved.[25] The fitting parameters of this last spectrum are shown in Table I. At 400 °C the sample again evolves towards ferromagnetism [Fig. 2(d)]. The further evolution at 500 °C annealing [Fig. 2(e)] shows a spectrum which can be interpreted as being mainly due to $Fe_4 N$ and α-Fe. We find a Fe/$Fe_4 N$ spectral area ratio of 0.37. All fitting parameters for this sample can be found in Table I.

Sample D ($P_{N2} = 3 \times 10^{-4}$ Torr) displays the CEMS spectra shown in Fig. 3. In the spectrum of Fig. 3(a) (as-deposited sample) we identify a broadened doublet due to ζ-$Fe_2 N$ together with a singlet attributable to γ-Austenite.[26] ζ-$Fe_2 N$ is incomplete. The sample remains practically in this condition up to 300 °C, Fig. 3(b). Note the change in the velocity scale. Phase transformations are visible after 400 °C annealing [Fig. 3(c)]. Finally at 500 °C annealing we obtain the spectrum 3c which is similar to spectrum 1c. This spectrum can be fitted and we identify again α-Fe together with γ'-$Fe_4 N$. It was impossible to meaningfully fit the internal part of the spectrum where a quadrupole doublet appears. This signal could correspond to $Fe_2 N$ or $Fe_3 N$ within an overwhelmingly ferromagnetic matrix. We find a relative spectral area of Fe/$Fe_4 N$ ratio of 0.66. Table I displays the fitting parameters.

B. X-ray diffraction results

The thin film structures have textures that do not display all diffraction lines which are present in bulk or powder samples. This makes the structural identification sometimes very difficult and sometimes ambiguous. By looking at the

TABLE I. Mössbauer fitting parameters of the three samples submitted to thermal treatment together with the identification of the phases and their relative spectral areas. (The isomer shifts are quoted with respect to Fe in Rh.)

Sample	$T(°C)$	Ident	H(kOe)	ΔE_Q	δ(mms^{-1})	Γ	%
B	as. Dep.	α-Fe	330	0	-0.10	0.38	59
		(?)	354.8	0.004	0.008	0.53	5
			226	0.10	0.21	0.87	36
	300	α-Fe	330	0	-0.11	0.25	41
		γ-Fe$_4$N	347	0.004	0.008	0.48	23
			229	0.105	0.22	0.67	36
	500	α-Fe	330	0	-0.10	0.24	60
		γ-Fe$_4$N	343	-0.06	0.15	0.30	
			217	-0.003	-0.17	0.31	40
C	as. Dep.		265	0	0.26	0.47	11
		Fe$_{2+x}$N	207	0	0.23	0.48	31
			179	0	0.20	0.42	4
			78	0	0.19	0.55	38
		Fe$_2$N	$\cdots$	0.87	0.26	0.58	1
			$\cdots$	0.47	0.30	0.35	15
	200	Fe$_2$N	$\cdots$	0.58	0.26	0.65	17
		Fe$_{2+x}$N	255.6	0	0.62	0.27	2
			196	0	0.25	0.71	51
			93	0	0.28	0.71	30
	300	ϵ-Fe$_2$N	$\cdots$	0.26	0.30	0.70	78
	300		58.6	0	0.29	0.65	22
	400	Fe$_2$N	$\cdots$	0.48	0.31	0.52	40
			64	0	0.34	0.60	60
	500	α-Fe	330	0	-0.09	0.29	27
		Fe$_4$N	345	0.05	0.14	0.43	
			217	0.02	0.29	0.37	73
D	as. Dep.	Fe$_2$N	$\cdots$	0.25	0.33	0.32	97
		γ-aust.	$\cdots$	0.29	0	0.27	3
	300	Fe$_2$N	$\cdots$	0.41	0.26	0.37	100
	400			Not fitted			
	500	α-Fe	329.5	-0	-0.10	0.24	43
		γ-Fe$_4$N	343	-0.017	0.15	0.27	
			217	0.03	0.18	0.36	52
		Fe$_2$N	$\cdots$	0.43	0.26	0.65	5

sequence of diffractograms of the present work the identification can be done with a reasonable amount of confidence. We compared our spectra with the JCPDS files.[27]

Figure 4 shows the thermal evolution of sample B ($P_{N2} = 4 \times 10^{-6}$ Torr). In the as-deposited condition, Fig. 4(a), we identify diffraction lines due to α-Fe, ζ-Fe$_2$N, and ϵ-(Fe$_2$N-Fe$_3$N) or γ'-Fe$_4$N which is barely visible. At 300 °C, Fig. 4(b), the heat treatment enhances the structure of γ'-Fe$_4$N together with α-Fe. The other compounds are slightly visible. This evolution continues at 400 °C [Fig. 4(c)] and seems to stabilize a mixture of predominantly γ'-Fe$_4$N together with some α-Fe at 500 °C, Fig. 4(d).

Sample C ($P_{N2} = 3 \times 10^{-5}$ Torr) pictured in Fig. 5 shows a rather different thermal evolution. The x-ray diffractogram shows mainly the hexagonal phase Fe$_3$N(H) with ζ-Fe$_2$N for the as-deposited sample, [Fig. 5(a)]. Originally we interpreted this Fe$_3$N(H) line as due to ϵ-Fe$_3$N,[21] but observing the evolution of this sample we can only assign this line to Fe$_3$N(H). Heat treating the sample at 300 °C [Fig. 5(b)] evidences the first signs of γ'-Fe$_4$N and a predominance of Fe$_3$N(H). We notice very little change at

400 °C. Finally at 500 °C γ'-Fe$_4$N is the only compound found in the diffractogram. α-Fe is absent in this whole picture. The Mössbauer result for this sample shows, nevertheless, that a small amount of α-Fe exists for the sample treated at 500 °C.

Finally sample D ($P_{N2} = 3 \times 10^{-4}$ Torr) shown in Fig. 6(a) (as-deposited) is a phase mixture of ζ-Fe$_2$N and ϵ-(Fe$_2$N-Fe$_3$N). There is no evidence of change up to 300 °C [Fig. 6(b)]. At 400 °C [Fig. 6(c)] the sample changes drastically towards a phase mixture of γ'-Fe$_4$N and α-Fe together with ϵ-(Fe$_2$N-Fe$_3$N) as a dominant diffraction peak. Finally at 500 °C [Fig. 6(d)] only γ'-Fe$_4$N and α-Fe remain, very much like sample B heat treated at 500 °C.

C. Magnetic measurements

In Fig. 7 we show the in plane hysteresis loops of the three samples after the 500 °C annealing. The magnetization axis is in arbitrary units. We note that all samples are ferromagnetic at room temperature. As-deposited, samples B and
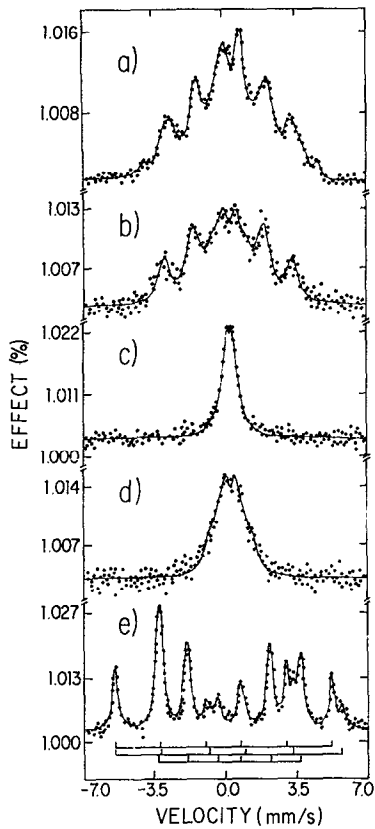
FIG. 2. Mössbauer results for sample C ($P_{N2} = 3 \times 10^{-5}$ Torr) (a) as-deposited; and annealed at: (b) 200 °C, (c) 300 °C, (d) 400 °C, (e) 500 °C.
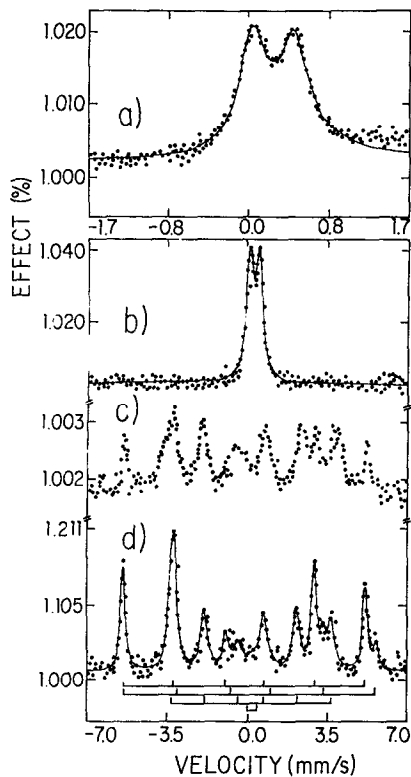

FIG. 3. CEMS spectra of sample D ($P_{N2} = 3 \times 10^{-4}$ Torr) Note tab. velocity change. (a) as-deposited; and annealed at: (b) 300 °C, (c) 400 °C, (d) 500 °C.
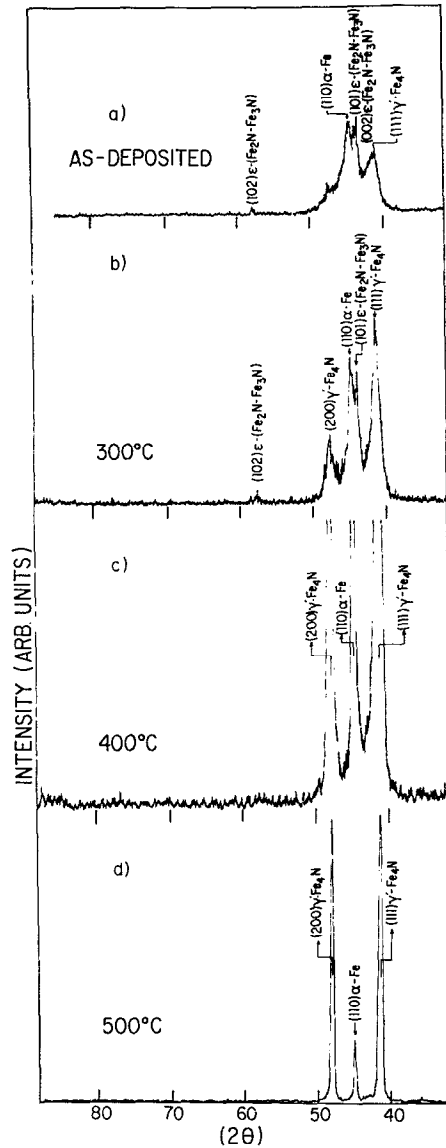

FIG. 4. X-ray diffraction results for sample B ($P_{N2} = 4 \times 10^{-6}$ Torr) (a) as-deposited annealed at: (b) 300 °C, (c) 400 °C, (d) 500 °C.

C were weakly ferromagnetic and sample D was paramagnetic down to 77 K. The annealed samples show two trends depending on the original nitrogen content in the sputtering chamber during deposition. First, we note that the coercive field increases with increasing P_{N2} : 51 Oe for sample B, 61 Oe for sample C, and 150 Oe for sample D, which was originally sputtered in a pure nitrogen ambient. Originally, samples B and C displayed coercive fields of 33 and 36 Oe, respectively. The coercivities found are below those reported for films obtained by IBAD,[8] and also below the particulate Fe₄N pigments.[2] But, in the pigments, the coercive field is mainly related to their acicular form. Second, we also find a squareness enhancement of the hysteresis loops as we go from sam-
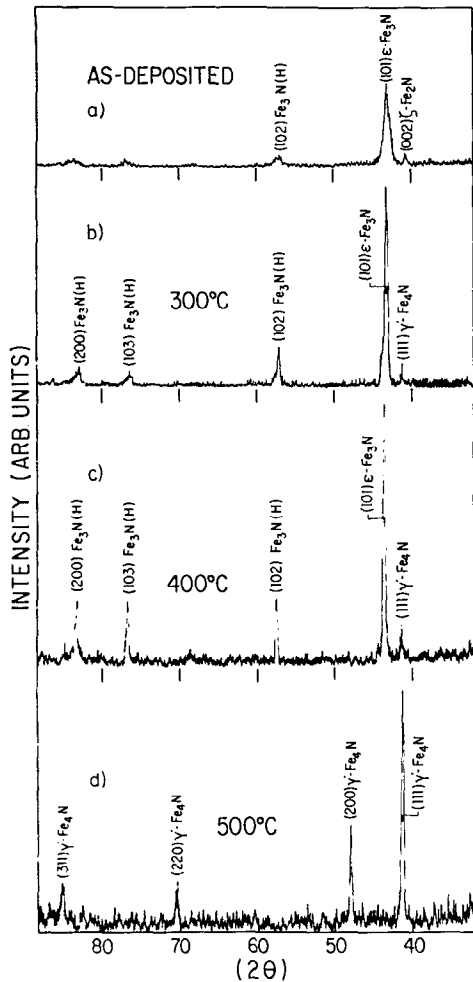
FIG. 5. X-ray spectra for sample C ($P_{N2} = 3 \times 10^{-5}$ Torr) (a) as-deposited annealed at: (b) 300 °C, (c) 400 °C, (d) 500 °C.
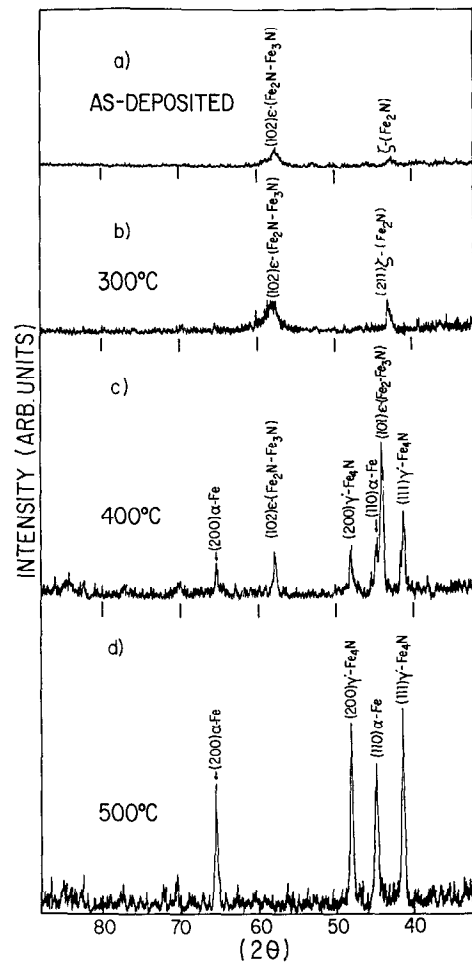

FIG. 6. X-ray diffraction results for sample D ($P_{N2} = 3 \times 10^{-4}$ Torr) (a) as-deposited annealed at: (b) 300 °C, (c) 400 °C, (d) 500 °C.

ple B to sample D. Sample D especially shows comparable saturation and remanent magnetizations. The squareness factor for this sample is 0.86, which is equal to the factor of acicular Fe_4N particulates.[8] Thus, all annealed samples show a much better squareness than pure iron films.

D. TEM characterization

Sample B ($P_{N2} = 4 \times 10^{-6}$ Torr) was also characterized as-deposited by transmission electron microscopy. We show bright-field, dark-field, and diffraction photographs in Fig. 8. The microstructure is markedly homogeneous. The dark-field picture shows a large number of fine grains with an average diameter of 400 Å. The diffraction picture characterizes the polycrystalline structure of ζ-Fe_2N.

IV. DISCUSSION AND CONCLUSIONS

The main experimental results are summarized in Table II, where the x-ray, CEMS, and magnetization findings are listed for the samples in the as-deposited and 500 °C annealed conditions.

As a general trend the reactively sputtered thin films rearrange under thermal treatment at 200–300 °C. The highly disordered phases transform themselves as interstitials and vacancies migrate. At still higher temperatures (starting at about 400 °C) the nitrides decompose and part of the nitrogen seems to leave the samples, since we now find the iron-rich phases. We identify γ'-Fe_4N and α-Fe in all samples. Of course only a significant change on the average stoichiometry can lead towards these results. This type of nitride decomposition is a well-known phenomenon in the iron surfaces nitrided by ion implantation[28] and also for bulk mate-
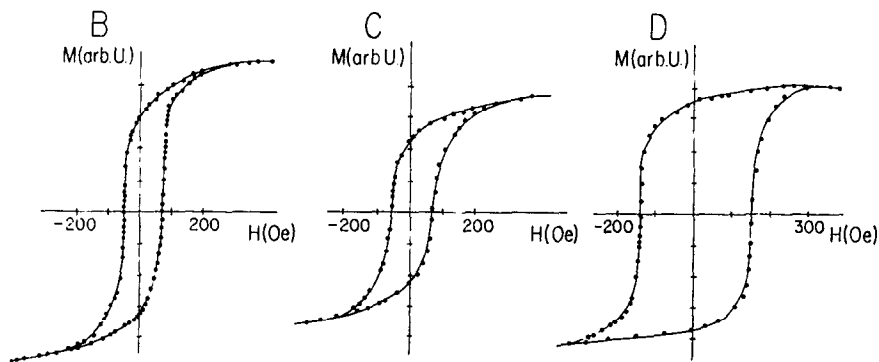
FIG. 7. Magnetization measurements for the three FeN_x samples after the 500 °C anneal. The hysteresis loops were obtained with the magnetic field in the plane of the thin films.
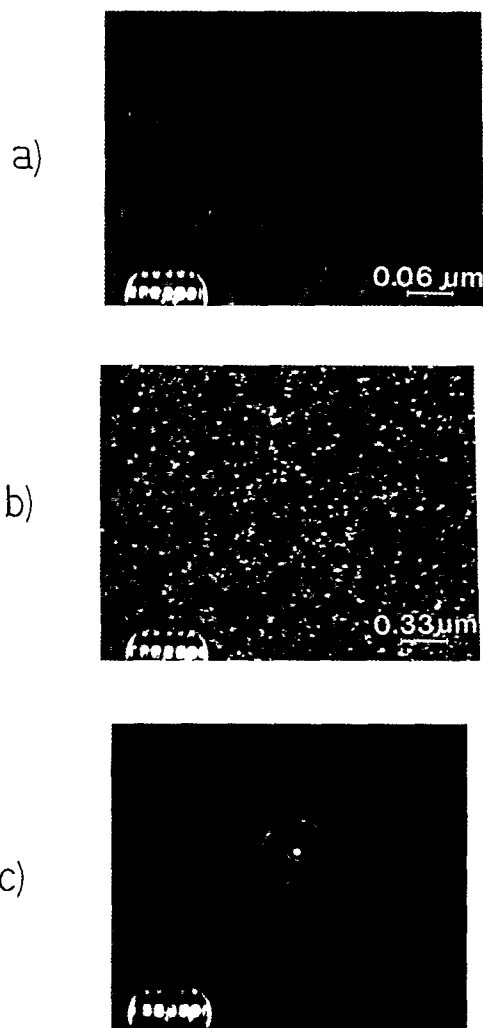

FIG. 8. Bright-field, dark-field, and diffraction pictures of the TEM characterization of sample B ($P_{N2} = 4 \times 10^{-6}$ Torr) as deposited.

rial.[29] What we note is that the decomposition temperature is some 100 °C lower for the thin film samples as compared to bulk samples.[30] This is not surprising since these sputtered films are fine grained, a fact which together with the typical thin film formation process of island coalescence and channel formation, should lower the decomposition temperature and promote out-diffusion of nitrogen.

One very interesting point to consider is the evolution of sample C ($P_{N2} = 3 \times 10^{-5}$ Torr) which has mainly γ'-$Fe_4 N$ with only a minor amount of α-Fe precipitation after the 500 °C anneal. This is in contrast with the two other samples. There has to exist a blocking mechanism which prevents the full α-Fe segregation. We note that the $Fe_3 N(H)$ phase is present only in this sample from the start and up to 400 °C. How this phase prevents the full α-Fe precipitation is, at present, unclear.

Having established that all samples evolve thermally towards the Fe-richer compounds, these are now much more interesting from the magnetic point of view than in the as-deposited condition. The magnetization measurements indeed show ferromagnetic behavior at room temperature for all samples. Especially sample D displays magnetic features which could turn out to be of interest for magnetic recording media. This sample has a high magnetization, since it is composed mainly of α-Fe and γ'-$Fe_4 N$, which have similar magnetizations,[8] apreciable squareness and remanence, a very steep switching field behavior, but still a somewhat moderate in plane coercive field. This higher coercivity of course has to arise out of the magnetic interplay of $Fe_4 N$ and Fe. The x-ray result for this sample after the 500 °C annealing shows that Fe is strongly textured and displays a different orientation with respect to the substrate as compared to sample B. This fact could increase the magnetic hardness. As the Mössbauer and x-ray results clearly show α-Fe and γ'-$Fe_4 N$ are present in all annealed samples in a wide range of relative proportions, but we find from the magnetic measurements that there exist certain $Fe/Fe_4 N$ proportions which promote magnetic quantities such as squareness and coercivity.

In summary we find a somewhat similar phase evolution in all iron nitride samples studied, independent of the origi-

TABLE II. Synoptic view of the starting and end products as characterized by x ray, CEMS, and magnetometry.

Sample	as-deposited			annealed at 500 °C		
	x ray	CEMS	VSM	x ray	CEMS	VSM
B	ζ-Fe$_2$N	α-Fe	fm	α-Fe	α-Fe(60%)	fm
$P_{N2} = 4\times10^{-6}$ Torr	ε-(Fe$_2$N-Fe$_3$N)	(?)	$H_c = 33$ Oe	γ'-Fe$_4$N	γ'-Fe$_4$N(40%)	$H_c = 51$ Oe
C	ζ-Fe$_2$N	Fe$_2$N	fm	γ'-Fe$_4$N	α-Fe(27%)	fm
$P_{N2} = 3\times10^{-5}$ Torr	Fe$_3$N(H)	Fe$_{2+x}$N	$H_c = 36$ Oe		γ'-Fe$_4$N(73%)	$H_c = 61$ Oe
D	ζ-Fe$_2$N	ε-Fe$_2$N			α-Fe(43%)	fm
		ζ-Fe$_2$N	param.	α-Fe	ε-Fe$_2$N(5%)	
$P_{N2} = 3\times10^{-4}$ Torr	ε-(Fe$_2$N-Fe$_3$N)			γ'-Fe$_4$N	γ'-Fe$_4$N(52%)	$H_c = 150$ Oe

nal nitrogen content. The relative proportions of each phase in the annealed samples is not given by the original nitrogen content. The nitrides evolve thermally according to the bulk phase diagram[30] but at significantly lower temperatures. After annealing, all samples show higher potential for recording media, especially sample D. We could not identify Fe$_{16}$N$_2$ at any stage of the evolution of these sputtered thin films.

This work will continue with the sputter-deposition of Fe/FeN$_x$ multilayers. The magnetic behavior of multilayers with different Fe/FeN$_x$ wavelengths is an interesting problem per se and the thermal evolution of these multilayers is expected to lead to very interesting results.

ACKNOWLEDGMENTS

[1] T. K. Kim, and M. Takahashi, Appl. Phys. Lett. 20, 492 (1972).
[2] A. Tasaki, K. Tagawa, E. Kita, S. Harada, and T. Kusunose, IEEE Trans. Magn. Magn. 17, 3026 (1981).
[3] K. Tagawa, E. Kita, and A. Tasaki, Jpn. J. Appl. Phys. 21, 1596 (1982).
[4] N. Saegusa, T. Tsukagoshi, E. Kita, and A. Tasaki, IEEE Trans. Magn. Magn. 19, 1629 (1983)
[5] S. Suzuki, H. Sakumoto, S. Miya, Y. Omote, and J. Minegishi, IEEE Trans. Magn. Magn. 20, 39 (1984).
[6] S. Susuki, H. Sakumoto, Y. Omote, and J. Minegishi, IEEE Trans. Magn. Magn. 20, 48 (1984).
[7] N. Terada, Y. Hoshi, M. Naoe, and S. Yamanaka, IEEE Trans. Magn. Magn. 20, 1451 (1984).
[8] K. Umeda, E. Kita, and A. Tasaki, IEEE Trans. Magn. Magn. 22, 591 (1986).
[9] M. Kume, T. Tsujioka, K. Matsuura, Y. Abe, and A. Tasaki, IEEE Trans. Magn. Magn. 23, 3633 (1987).
[10] H. De Rugy, J. P. Langeron, S. Bouquet, L. Minel, G. I. Grigorov, and I. N. Martev, Thin Solid Films 161, L69 (1988).
[11] M. Nagakubo, T. Yamamoto, and M. Naoe, J. Appl. Phys. 63, 4309 (1988).
[12] J. Lo, L. Franco, T. C. Huang, T. W. Wu, D. Miller, and R. Campbell, IEEE Trans. Magn. Magn. 24, 3081(1988).
[13] M. Naoe, M. Nagakubo, and T. Yamamoto, J. Appl. Phys. 64, 5449 (1988).
[14] M. Kume, S. Takahashi, T. Tsujioka, K. Matsuura, and Y. Abe, IEEE Trans. Magn. Magn. 24, 3003 (1988).
[15] P. Chatterjee and A. K. Batabyal, Thin Solid Films 169, 79 (1989).
[16] K. Nakajima and S. Okamoto, Appl. Phys. Lett. 54, 2536 (1989).
[17] A. Kano, N. S. Kazama, and H. Fujimori, J. Appl. Phys. 53, 8332 (1982).
[18] C. Lo, S. V. Krishnaswamy, R. Messier, K. R. P. M. Rao, and L. N. Mulay, J. Vac. Sci. Technol. 18, 313 (1981).
[19] C. Lo, S. V. Krishnaswamy, L. N. Mulay, and R. A. Diffenbach, J. Appl. Phys. 53, 2745 (1982).
[20] C. Chang, J. M. Sivertsen, and J. H. Judy, IEEE Trans. Magn. Magn. 23, 3636 (1987).
[21] D. H. Mosca, P. H. Dionisio, W. H. Schreiner, I. J. R. Baumvol, and C. Achete, J. Appl. Phys. 67, 7514 (1990).
[22] N. De Cristofaro and R. Karplow, Metall. Trans. A 8, 35 (1977).
[23] P. Rochegude, and J. Foct, Phys. Status Solidi (A) 98, 51 (1986).
[24] M. Mekata, H. Yoshimura, and H. Takoki, J. Phys. Soc. Jpn., 33, 62 (1972).
[25] M. Chabanel, C. Janot, and J. P. Motte, C. R. Acad. Sci. Paris B 226, 419 (1968).
[26] N. E. W. Hartley, Thin Solid Films 64, 177 (1979).
[27] Powder Diffraction File Search Manual (JCPDS, Swarthmore, PA, 1978).
[28] C. A. dos Santos, B. A. S. de Barros Jr., J. P. de Souza, and I. J. R. Baumvol, Appl. Phys. Lett. 41, 237 (1982).
[29] Yu. V. Maksimov, I. P. Suzdalev, M. Ya. Kushnerev, and R. A. Arents, Fiz. Metal. Metalloved. 37, 267 (1974).
[30] O. Kubaschewski, Iron-Binary Phase Diagrams (Springer, New York, 1982), p. 67.